Experimental Based Evaluation of PV Inverters Harmonic and Interharmonic Distortion Due to Different Operating Conditions

Experimental Based Evaluation of PV Inverters Harmonic and Interharmonic Distortion Due to Different Operating Conditions

R. Langella (*), *Senior Member IEEE*, A. Testa (*), *Fellow IEEE*, J. Meyer (**), *Member, IEEE,*
F. Möller (**), R. Stiegler (**), S. Z. Djokic (***), *Senior Member IEEE*

(*) Second University of Naples, Aversa (CE), Italy (roberto.langella@unina2.it; alfredo.testa@unina2.it)
(**) Technische Universitaet Dresden, Germany (jan.meyer@tu-dresden.de, friedemann.moeller@tu-dresden.de, robert.stiegler@tu-dresden.de)
(***) University of Edinburgh, Scotland, U.K. (sasa.djokic@ed.ac.uk)

Abstract—**This paper presents the results of comprehensive testing, and subsequent detailed analysis of obtained test results, evaluating harmonic and interharmonic performance of PV inverters (PVInvs) for a range of different operating conditions. The presented results indicate significant power-dependent changes in harmonic and interharmonic emissions of tested PVInvs for different supply voltage conditions (presence of voltage waveform distortions and various source impedance values). To correctly quantify and describe these changes in PVInvs' performance, the paper discusses and applies measurement procedures and metrics for evaluating harmonic and interharmonic emission recommended in existing standards, as well as some additional metrics and indicators. For some operating conditions, tested PVInvs significantly increase both harmonic and interharmonic emission, and paper also discusses impact of PVInvs' controls (e.g. maximum power point tracking control) as a possible origin of the interharmonic distortion.**

Keywords—Harmonic and Interharmonic Distortion; Measurement Procedures; Operating Conditions; Photovoltaic Inverter, Power Quality.

I. INTRODUCTION

Numbers and sizes of solar photovoltaic (PV) installations are steadily increasing, mainly as a result of reduced PV panel costs and various efforts and incentives (e.g. feed-in tariffs) aimed at reducing CO2 and other GHG emissions from the power generation sector. It is expected, for example, that the total worldwide solar PV capacity will grow from around 2% in 2012 to around 16% by 2030, as both the recent and projected cost reductions and efficiency improvements should make PV-based electricity generation (particularly in the case of larger PV systems) cost-competitive with conventional power sources [1].

For their connection to the grid, PV generation systems require a power electronic interface, which is typically a dc-ac inverter implementing pulse-width modulated (PWM) control and filtering circuits for both conversion of input dc currents/voltages and regulation of output ac currents/powers. Due to dc-ac conversion, one important requirement for PV inverter (PVInv) operation is to ensure compliance with specified harmonic emission limits, e.g. those in [2].

It is generally expected that modern PVInvs will have (very) low harmonic emissions, which should be verified in direct equipment tests. For testing, [2] acknowledges that harmonic and interharmonic emission of PVInvs might increase for lower than rated power outputs and that the presence of voltage supply distortions might have an additional impact on PVInv harmonic performance. However, [2] also suggests that testing of PVInvs should be performed with their power outputs adjusted at 25%, 50% and 100% of rated powers, although the outputs of any PVinv can be, and typically are often lower, based on variations of daily solar irradiance and cloud coverage conditions, e.g. [3].

This paper builds on the initial results and analysis presented in [4], which are extended by providing both the additional results of testing and measurements, as well as the further analysis and investigation of the changes in harmonic and interharmonic performance of PVInvs for different operating powers and for different voltage supply conditions. Of particular importance are notable changes of PVInvs' performance in low-power operating modes, which cannot be identified if their minimum power output during the tests is set at 25%, as recommended by [2] (e.g. in [5]). The paper discusses and applies measurement and calculating procedures recommended in current standards for evaluating harmonic and interharmonic contents and corresponding distortion levels (e.g. in [6]), and also introduces some further metrics and indicators. Finally, the paper investigates the impact of PVInvs' controls as a possible reason for the increased harmonic and interharmonic distortion. Particular attention is given to the analysis of the impact of maximum power point tracking (MPPT) control, which is responsible for the increased variations of input dc voltages in low-power operating modes, becoming particularly pronounced in very low-power operating modes, due to the increased "flatness" of P-V curve of the connected panels. It is found that the MPPT control is likely origin/cause of the increased PVInvs interharmonic emission which, to the best of the authors' knowledge, is so far not reported in existing literature.

II. Experimental Set-Up and Tested PV Inverters

As the numbers and sizes of installed PV systems increase, it is important to correctly represent their power-dependent harmonic and interharmonic characteristics for the analysis of their impact on the operation of LV and MV networks. One recent example that documents a nuisance tripping of power protection systems due to the increased PVInvs' harmonic emissions in low-power mode is discussed in [7].

Three different PVInvs were subjected to a comprehensive laboratory testing and measurement campaign, in which their adjusted power outputs were varied in a range from the rated/nominal power to the minimum possible power at which they were able to maintain stable operating points.

A. Test Set-Up

The test set-up, whose simplified scheme is reported in Fig. 1, consisted of a i) PV Emulator [8]; ii) a three-phase programmable Power Amplifier [9] including a programmable Line Impedance model [10]; iii) a Data Acquisition system [11]; iv) a connection control panel, and v) the tested PVInvs. The output of PVInvs was connected directly to the Power Amplifier (to dissipate generated power) and specific combinations of test voltage waveforms and source impedances are pre-programmed. The test procedure has been automatic controlled by the Control PC.

The main characteristics of the test set-up are:

- PV Emulator: free programmable I/V characteristics, fast response time to load changes typical less than 100µs, Voltage accuracy at MPP of ± 2 V, Current accuracy at MPP of ± 0.25 A, P_{rated} = 10 kW.
- Power Amplifier: Vertical resolution: (± 32,768 points), Horizontal resolution (per cycle) 1,024 points, Amplitude resolution: 0.01 %, Voltage accuracy: <0.1 %, Voltage offset: <1 mV, P_{rated} = 45 kVA.
- Data acquisition system. Signal conditioning modules: voltage and current modules ([12]-[13]) are equipped with a 3rd order low pass Butterworth filter, which has been set to 100 kHz (-3 dB) in order to eliminate aliasing effects; voltage were directly measured setting the measurement range to ±400 V and ±800 V for ac and dc channels, respectively while current measurements were performed using flux compensated Hall-element clamps with a full scale of 150 A and setting the measurement ranges for ac and dc channels to1 V/50 A and 0.5 V/25 A, respectively. DAQ board: 2x8 synchronous analog inputs with a 16-bit resolution and maximum sampling rate per channel of 1 MHz (the used sampling rate was 300 kHz).

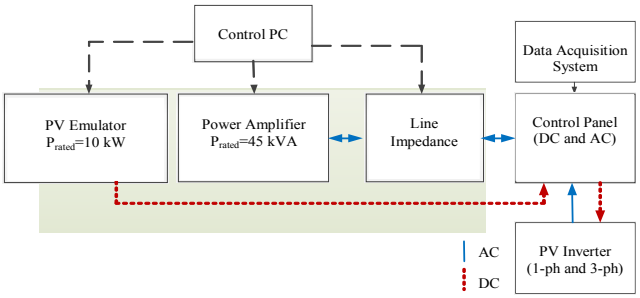

Fig. 1. Simplified scheme of the fully automated test set-up.

B. Uncertainty Analysis of the Current Measurement Chain

The combined standard uncertainty of the current measuring chain is determined by Monte Carlo (MC) simulations [14], starting from the standard uncertainties of the used current clamps, of the signal conditioning module and of the ADC. As the uncertainties specified in the measurement equipment datasheets apply for the sampled values, MC simulations have been performed to determine how the uncertainty in time domain propagates to the harmonics in frequency domain.

Fig. 2. shows, for each trial of the MC simulation, the algorithm implemented. First, input data (amplitudes, frequencies and phase angles) for the reference signal, consisting of a fundamental component (I_1, f_1, ϕ_1) and one harmonic component (I_h, f_h, ϕ_h), are set. Then, for each time sample k/f_s (where f_s is the sampling frequency), the reference signal sample is generated in time-domain. At each stage of the measurement chain, a random measurement deviation value, based on the datasheet specifications, is generated using a standard rectangular distribution. The three deviation values are then added to the signal which is buffered. Once the number of samples corresponding to ten periods of the fundamental ($10 \cdot f_s/f_1$) is buffered, a DFT is performed and the calculated harmonic amplitude, $\hat{I}_h$, is compared with the reference one, I_h, obtaining its deviation.

The following standard uncertainties have been used:

- Current clamps (output sensitivity: 20 mV/A): ±1 % of reading ±2 mA up to 100 kHz (-1 dB) [15] ;
- Signal conditioning: ±0.4 % of reading ±0.5 mV up to 50 kHz [13];
- ADC: ±0.02 % of reading ±0.65 mV up to 900 kHz [16].

For frequencies up to 50 kHz, current transducers, which are the main cause of inaccuracy [17], have been carefully characterized and opportune compensation factors have been used for taking into account systematic effects.

The total of 50,000 Monte Carlo trials have been performed in order to get a representative set of results. As an example, Fig. 3 shows the pdf of the amplitude deviation for the 11th harmonic, characterized by an amplitude of 100 mA, together with the fitted normal distribution. The assumption of the normal distribution is confirmed by applying the Anderson-Darling goodness-of-fit test [18]. It should be noted that the expanded standard uncertainty with a coverage factor 6 is equal to 1.9%, while it is equal to 0.96% with a coverage factor 3.

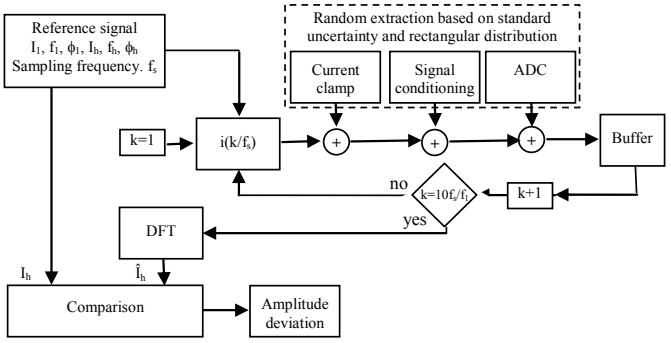

Fig. 2. Algorithm implemented for each trial of the MC simulation.

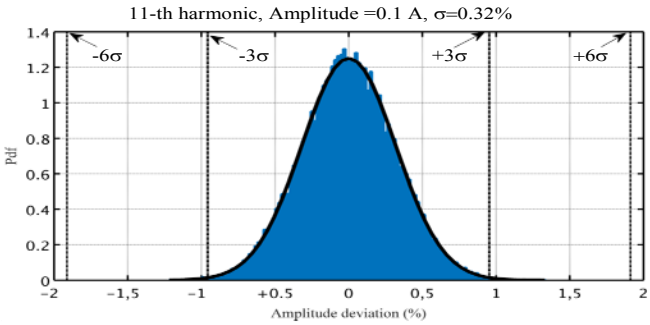

Fig. 3. PDF of amplitude deviation for the 11th harmonic with 100 mA rms magnitude (blue) and the fitted normal distribution (black)

Fig. 4 shows the expanded uncertainty values, with a coverage factor equal to 3, for five selected harmonics with different amplitudes. The expanded uncertainty is decreasing with increasing amplitude and almost independent of the harmonic order up to 50 kHz. As expected, the calculated level of confidence was in the range 99.66-99.78%.

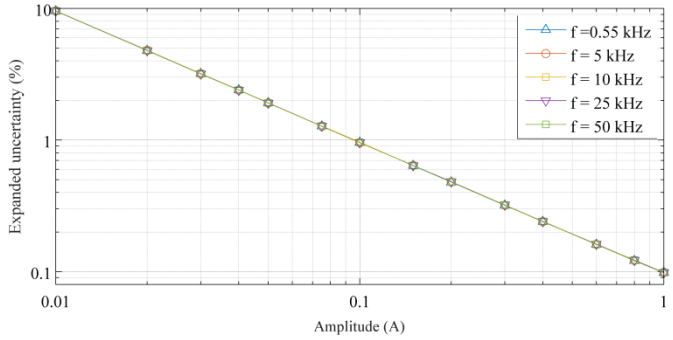

Fig. 4. Expanded uncertainty (3σ) vs. harmonic magnitudes and orders.

The following combined standard uncertainties could be derived from the previous analysis:

- Less than 3.2% for magnitudes higher than 10 mA;
- Less than 0.63% for magnitudes higher than 50 mA;
- Less than 0.33% for magnitudes higher than 100 mA;
- Less than 0.17% for magnitudes higher than 200 mA.

The combined standard uncertainty of the calculated total harmonic current values can be determined by the combined standard uncertainties of the rms values of the individual harmonics [19]. If one harmonic magnitude dominates the THC, its uncertainty corresponds approximately to the individual uncertainty of the respective harmonic. As often only one low order harmonic (in most cases the 3rd harmonic) usually dominates the total harmonic current of PVinvs, for THC values the same combined standard uncertainties for single components can be assumed as realistic estimate for most cases.

C. *Tested PV Inverters*

Table I lists the basic data for the three tested PVInvs.

TABLE I. BASIC PV INVERTER CHARACTERISTICS.

Characteristic	PV inverter Notation		
	PVInv-A	PVInv-B	PVInv-C
Rated power, kVA	4.6	10	4.6
Phase connection	1-phase	3-phase	1-phase
Topology	Transformerless	HF transformer	LF Transformer

D. *Operating Conditions Applied in Tests*

The analysis of the possible ranges of variations of harmonic and interharmonic characteristics for different LV supply conditions and various PVInv operating conditions is assessed with respect to the three main test parameters:

a) source impedance value, which was adjusted in accordance to [20] as either the minimum possible source impedance, ZS1~0 (due to only impedances of a cable connecting PVInv to the power amplifier and power amplifier itself), representing a strong grid, or the maximum expected LV network source impedance (at 90% of supply points), consisting of Z_{phase} = (0.24+j0.15) Ω for phase conductor(s) and $Z_{neutral}$ = (0.16+j0.10) Ω for neutral conductor, ZS2 = (0.4+j0.25) Ω, representing a weak grid.

b) presence of waveform distortions in ac supply voltage (so called "background distortion"), which was emulated first as ideally sinusoidal waveform (WF1), and then with two typically distorted voltage waveforms (WF2 and WF3).

c) input power of tested PVInvs, which was adjusted by PV emulator to the following values of solar irradiance (SI): 100%, 75%, 50%, 25%, 20%, 15%, 10% and 5% of the nominal SI value (1,000 W/m^2), corresponding to PVInv's rated power.

The three test supply voltage waveforms are shown in Fig. 2 and specified in Table A.I in Appendix A. WF1 represents a reference, i.e. an ideally sinusoidal voltage waveform. The two distorted waveforms are derived from the measurements in LV networks. The "flat-top" distorted WF2 is typical for a large number of residential customers with 2-pulse rectifiers, while the "pointed-top" distorted WF3 is typical for LV networks with a large number of industrial customers with 6-pulse rectifiers. All measurements (and further processing of measured results) have been performed in accordance with the relevant recommendations in [6] and [21]. The corresponding values for the total harmonic distortion (THD) and crest factor (CF) are also provided in the legend of Fig. 5.

Accordingly, each PVInv is tested with the minimum of the 48 different test points, corresponding to the combinations of three main test parameters listed in Table II.

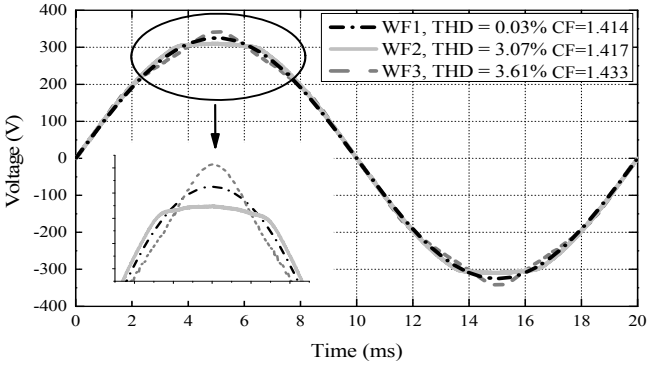

Fig. 5. The three supply voltage waveforms used in tests.

TABLE II. SPECIFICATION OF TEST PARAMETERS.

Parameter	Adjusted Values	Test Points
Source Impedance	ZS1~0, ZS2=(0.4+j0.25) Ω	2
Waveform Distortion	WF1, WF2, WF3	3
Power output (Input Solar Irradiance)	100%, 75%, 50%; 25%, 20%, 15%, 10%, 5%	8

III. General Harmonic and Interharmonic Evaluation Framework

The IEC standard [6] defines signal processing methods and calculation methods for harmonic and interharmonic measurements and analysis. It recommends a time window for spectral analysis of exactly 10 periods of the supply system frequency in 50 Hz systems and 12 periods in 60 Hz systems, corresponding to about 200 milliseconds and to the frequency resolution of about 5 Hz. The standard covers the "classical" low-frequency (LF) range from 0 to 2 kHz (up to the 40th harmonic order in 50 Hz systems) and contains an informative annex regarding the frequency range from 2 kHz to 9 kHz (up to the 180th harmonic order in 50 Hz systems).

In order to assess the cumulative distortion, for Class A instruments, [6] suggests the use of the Subgroup Total Harmonic Distortion ($THDS_Y$) factor, which is expressed as a relative, i.e. percentage harmonic distortion in LF range with respect to the fundamental subgroup. In this paper, this is referred to as $THDS_{YLF}$ ($THDS_Y$ in Low-Frequency range):

$$THDS_{YLF} = \sqrt{\sum_{h=2}^{h=40}\left(\frac{Y_{sg,h}}{Y_{sg,1}}\right)^2} \quad (2)$$

where: the symbol *Y* is replaced, as required, by the symbol I for currents, or by the symbol *U* for voltages; $Y_{sg,1}$ and $Y_{sg,h}$ are the rms magnitudes of the fundamental and harmonic subgroups in the low-frequency range, from 0 - 2 kHz.

In [6] and [21], no reference is explicitly made to the Subgroup Total Interharmonic Distortion (TIHDS) factor, but in existing literature and in some of the commercial PQ instruments, complying with Class A requirements from [21], reference is made to the following $TIHDS_{YLF}$ formulation:

$$TIHDS_{YLF} = \sqrt{\sum_{h=2}^{h=40}\left(\frac{Y_{isg,h}}{Y_{sg,1}}\right)^2} \quad (2)$$

where $Y_{isg,h}$ are the rms magnitudes of the interharmonic subgroups in the low-frequency range, from 0 - 2 kHz.

Finally, in order to give some information about the distortions at higher frequencies, which are not considered in [6], the authors introduced the following Subgroup Total Harmonic and Interharmonic Distortion ($TH\&IHDS_{YHF}$) factor in high-frequency (HF) range, based on the notion that for higher frequencies no conceptual differences exist between harmonics and interharmonics:

$$TH\&IHDS_{YHF} = \sqrt{\sum_{h=41}^{h=1000}\left[\left(\frac{Y_{sg,h}}{Y_{sg,1}}\right)^2 + \left(\frac{Y_{isg,h}}{Y_{sg,1}}\right)^2\right]} \quad (3)$$

This index extends the concepts suggested in Annex B (informative) of [6] for measurements in the frequency range 2kHz-9kHz to the high-frequency range from 2kHz to 50kHz; moreover, it is worthwhile noting that (3) is perfectly coherent with the 200 Hz bands grouping concept introduced in the Annex of [6], once the band pass filtering with attenuation of the fundamental component of at least 55 dB is applied.

The numerators of (1)-(3) give harmonic and interharmonic distortions in absolute values (in amperes) and are denoted as $THCS_{YLF}$, $TIHCS_{YLF}$ and $TH\&IHCS_{YHF}$.

IV. Impact of Different Solar Irradiation Levels and Grid Conditions

In accordance with standards (e.g. [2]), each adjusted SI value was kept constant in tests for at least 1 minute, in order to allow PVInv to reach steady state operating conditions. In practice, however, PV systems are typically exposed to dynamic changes of input SI, e.g. due to short-term variations in cloud coverage conditions, which could vary in a wide range, regarding both actual SI levels and transitions between them. Although none of existing standards specifies testing of PVInvs for dynamic changes in SI, one such example is shown here in order to illustrate further differences in PVInv's performance with respect to steady state operating conditions.

Fig. 6 compares dynamic and steady state harmonic and interharmonic performance of PVInv-B. A continuous linear reduction of input SI is adjusted over the period of 30 seconds, starting from 1,000 W/m^2 down to the very low SI level of 50 W/m^2. The experiment ended by the tripping of PVInv around five seconds after a low SI level was reached, as inverter's control was not able to maintain further operation in a very low-power mode. The corresponding dynamic values of $THDS_{ILF}$ (Fig. 6a, blue line) and $TIHDS_{ILF}$ (Fig. 6b, blue line) are calculated from the output ac supply current and compared with corresponding steady state $THDS_{ILF}$ and $TIHDS_{ILF}$ values (marked with a "star" symbol), obtained in separate steady-state tests.

Fig. 6 clearly shows that although there are very small differences between the dynamic and steady state results for higher SI levels, the tripping of PVInv and significant increase of dynamic $THDS_{ILF}$ and, particularly, dynamic $TIHDS_{ILF}$ values for very low SI levels (4-5 times), is another important aspect required for a full assessment of PVInv performance. Although the tests with dynamic SI changes are not considered further in this paper, it is worth noting that these tests could be used as a basis for an additional immunity testing of PVinvs (e.g. [22]), which could be denoted as a "cloud-ride-through" testing of PVInv.

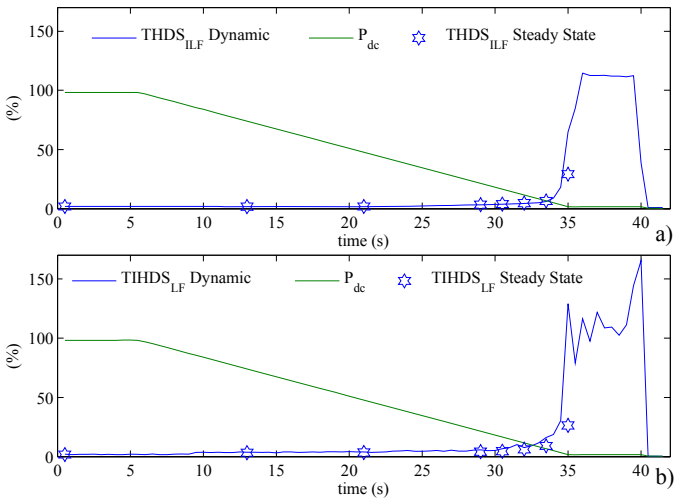

Fig. 6. Comparison of the dynamic and steady state responses of PVInv-B for continuously reduced and fixed SI levels (in percentage of nominal 1,000 W/m^2): a) $THDS_{ILF}$; b) $TIHDS_{ILF}$.

The following sub-sections present the results of the comprehensive tests of three PVInvs for steady state operating conditions. Based on the uncertainty analysis presented in Subsection II.B, it was verified that the combined standard uncertainty does not affect significantly the generality of the considerations reported in the following text. Moreover, the presented results are consistent with similar results reported in the relevant literature. For these reasons and due to a large number of curves in the following figures, the ±3σ curves have not been plotted.

A.PV Inverter A

Relative and absolute distortion factors of PVInv-A for the specific combinations of test voltage waveforms and source impedances are illustrated in Figs. 7 and 8.

Fig. 8a is of particular importance for evaluating power-dependency of harmonic emission of PVInv-A in LF range (0 - 2 kHz), as it demonstrates that the significant increase of relative harmonic emission (i.e. calculated $THDS_{ILF}$ values in Fig. 7a) is not only due to the reduced fundamental currents in very low-power operating mode, i.e. reduced denominator in (1). After an initial decrease, the $THCS_{ILF}$ values in amps of PVInv-A (Fig. 8a) actually start to increase with decreasing power in the low-power operating modes, reflecting significant change in its behavior, and almost matching the $THCS_{ILF}$ values in amps at the higher operating powers. Consequently, $THDS_{ILF}$ values for WF1 and ZS1 in very low power mode increase almost 50 times (at 5% SI level, $THDS_{ILF}$ is around 100%).

Power-dependent interharmonic emission of PVInv-A in LF range is similar to its power-dependent harmonic performance. Relative interharmonic distortion (quantified by $TIHDS_{ILF}$ values in Fig. 7b), increases almost 30 times in very low power mode, compared to its $TIHDS_{ILF}$ value at rated power. After an initial decrease with reduced power outputs, $TIHCS_{ILF}$ values in amps (Fig. 8b) in low-power operating modes remain constant or slightly increase, approaching $TIHCS_{LF}$ values at the higher operating powers.

Both Fig. 7 and Fig. 8 demonstrate significant impact of the combined effects of supply voltage distortions ("flat-top" and "pointed-top" background distortions, WF2 and WF3) and maximum expected source impedance, ZS2, on relative and absolute harmonic emissions in LF range (up to a five-fold increase for most of operating powers), as already reported in [23]. The impact of only high source impedance without background distortion (i.e. results for WF1 and ZS2) in LF range, however, is more complex. PVInv-A reduces its relative and absolute harmonic emission, but increases its relative and absolute interharmonic emission, compared to the results with sinusoidal supply and no source impedance (WF1 and ZS1).

In the considered HF range (2 kHz - 50 kHz), PVInv-A reduces its harmonic and interharmonic emissions for ZS2 and all waveforms with respect to the results with ZS1 and WF1, due to the strong damping effects of the introduced high value of the source impedance (Figs. 7c and 8c).

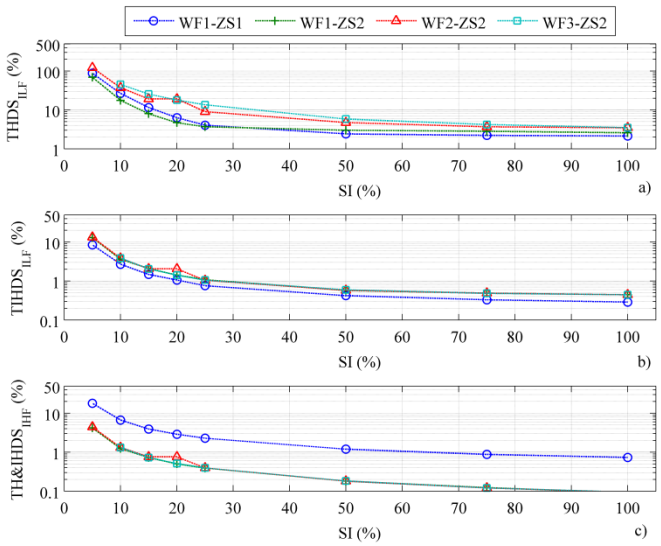

Fig. 7. PVInv-A relative distortion factors for selected combinations of test voltage waveforms and source impedances: $THDS_{ILF}$, b) $TIHDS_{ILF}$ and c) $TH\&IHDS_{IHF}$.

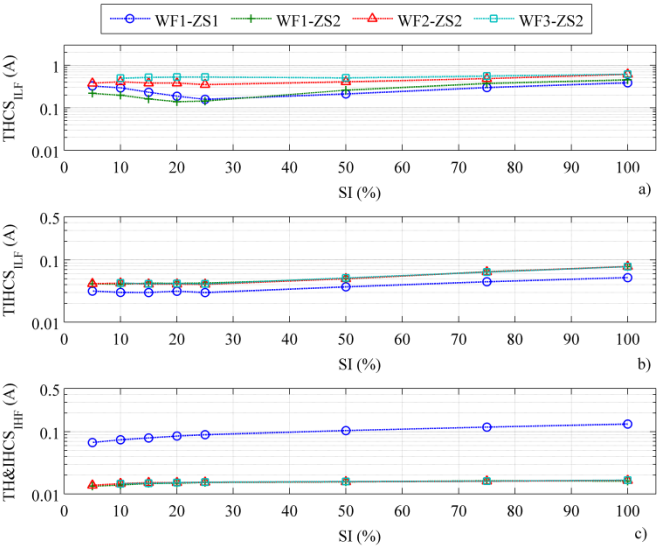

Fig. 8. PVInv-A absolute distortion factors (in Ampere) for selected combinations of test voltage waveforms and source impedances: a) THCSILF, b) TIHCSILF and c) TH&IHCSIHF.

B.PV Inverter B

Figs. 9 and 10 illustrate the results of testing of PVInv-B. The results for WF1 and ZS1 show that the increase of relative harmonic distortion in very low power mode is around 15 times (at 5% SI, $THDS_{ILF}$ is around 30%, compared to around 2% at 100% SI), while $THCS_{ILF}$ value at 5% SI is close to the $THCS_{ILF}$ value at SI of 50%. There is again strong impact of waveform distortions and source impedance on relative harmonic emission of PVInv-B: $THDS_{ILF}$ values for WF2 and WF3 for ZS2 exhibit further increase of around 15 times, reaching 500% at SI of 5%. Power-dependent $THCS_{ILF}$ values for WF2, WF3 and ZS2 also significantly increase and are not dependent on operating power (Fig. 10a). The impact of introducing only high source impedance (ZS2) without background distortion (for WF1) in LF range for PVInv-B is very small.

The results in Fig. 9b show that relative interharmonic distortion of PVInv-B starts to increase in low power mode and in very low power mode becomes around 20 times higher than at rated power. Highest interharmonic emission in amps (Fig. 10b) is at around 75% of its rated power, while power-dependent changes are again visible in high, low and very low operating modes. As for harmonic and interharmonic emission in HF range, the strong damping effects of the introduced high source impedance (ZS2) is again evident for PVInv-B.

It is interesting to note that for WF1 and ZS1 and based on operating power, absolute harmonic and interharmonic emission of PVInv-B in HF range (Fig. 10c) is either higher than, or comparable to the corresponding absolute harmonic and interharmonic emissions in LF range.

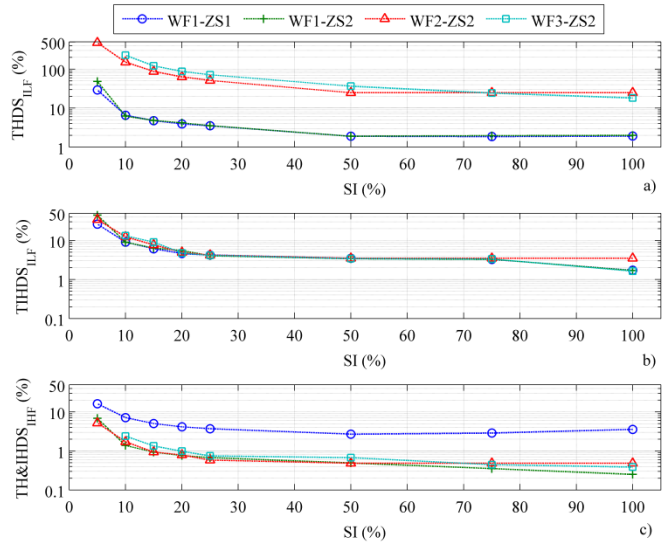

Fig. 9. PVInv-B relative distortion factors for selected combinations of test voltage waveforms and source impedances: a) $THDS_{ILF}$, b) $TIHDS_{ILF}$ and c) $TH\&IHDS_{IHF}$.

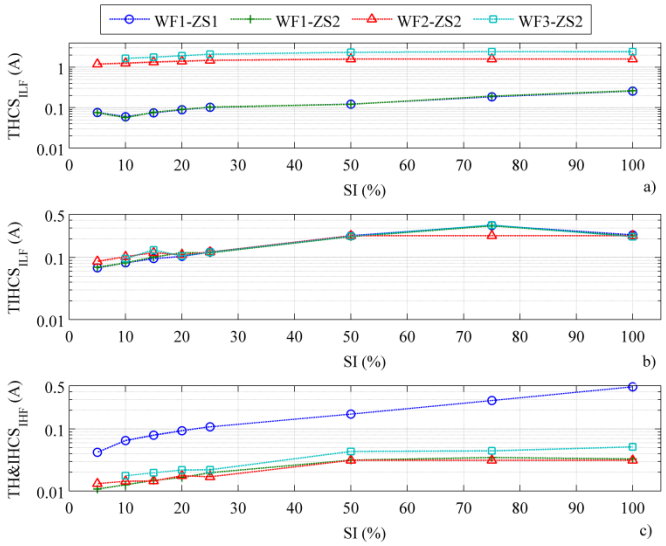

Fig. 10. PVInv-B absolute distortion factors (in Ampere) for selected combinations of test voltage waveforms and source impedances: a) $THCS_{ILF}$, b) $TIHCS_{ILF}$ and c) $TH\&IHCS_{IHF}$.

C. PV Inverter C

The results of testing PVInv-C in Figs. 11 and 12 show that its relative harmonic distortion for WF1 and ZS1 at SI of 5% is around 10 times higher than at SI of 100% (Fig. 11a). However, as the adjusted power output of PVInv-C reduces, its absolute harmonic emission (Fig. 12a) is continuously decreasing, although there are visible changes in the gradient of the line that connects plotted $THCS_{ILF}$ values between high, low and very low power operating modes.

At all operating powers, the presence of waveform distortions and source impedance (WF2 and WF3 for ZS2) results in 2-3 times higher relative and absolute harmonic emissions than for the WF1 and ZS1.

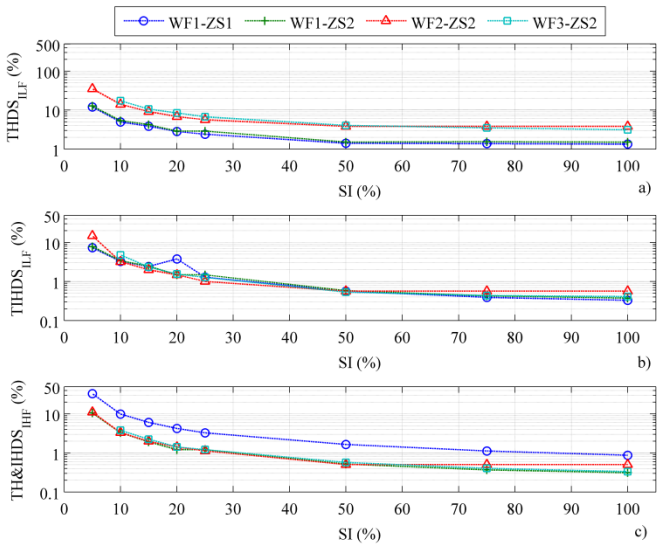

Fig. 11. PVInv-C relative distortion factors for selected combinations of test voltage waveforms and source impedances: a) $THDS_{ILF}$, b) $TIHDS_{ILF}$ and c) $TH\&IHDS_{IHF}$.

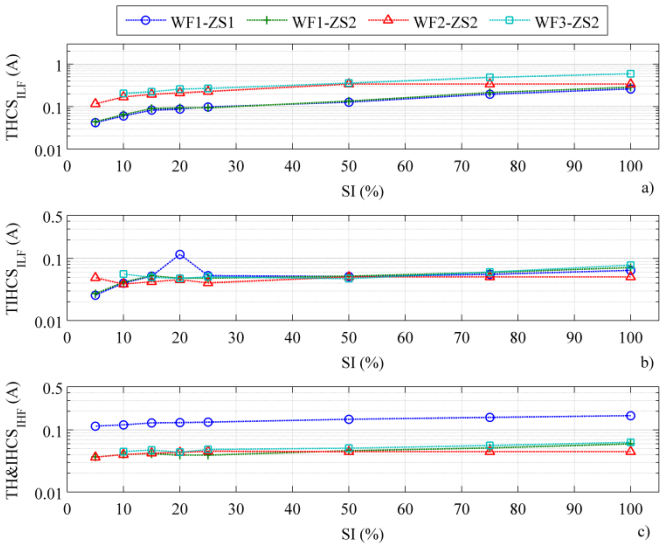

Fig. 12. PVInv-C absolute distortion factors (in Ampere) for selected combinations of test voltage waveforms and source impedances: a) $THCS_{ILF}$, b) $TIHCS_{ILF}$ and c) $TH\&IHCS_{IHF}$.

Figs. 11b and 12b indicate that the highest absolute interharmonic emission ($TIHCS_{ILF}$ in amps) for PVInv-C is again not at rated power, but it is in the low power operating mode (around 20% of its rated power). Relative interharmonic distortion at 5% SI is around 20 times higher than the distortion at 100% SI. Impact of waveform distortions and source impedance on both relative and absolute interharmonic distortions is very small.

In HF range, the results for harmonic and interharmonic emission again confirm strong damping effects of the introduced high source impedance (ZS2). Similarly to PVInv-B, absolute harmonic and interharmonic distortion of PVInv-C in HF range (Fig. 12c) is either higher than or comparable to its harmonic and interharmonic distortions in LF range.

D. Discussion of Test Results for All PV Inverters

The results of comprehensive tests in previous sub-sections demonstrate significant power-dependent changes in harmonic and interharmonic emission of all three tested PVInvs. The presence of supply voltage waveform distortion and source impedance has an additional strong impact on these changes, which effectively required to use logarithmic scale for Y-axes in Figs. 7-12, in order to cover the full ranges of values of the presented harmonic and interharmonic distortion indices.

The presented results for LF range (0 - 2 kHz) indicate complex harmonic and interharmonic performance of all three tested PVInvs, with noticeable differences in their behavior. In HF range (2 kHz - 50 kHz), however, all three PVInvs exhibit the same characteristics due to strong damping effects of the source impedance used in tests. This is discussed in the further text, where harmonic and interharmonic distortion indices for PVInvs operating at rated power (for SI=100%) and connected to ideally sinusoidal supply with no source impedance (for WF1 and ZS1) are used as the reference values.

1) LF harmonics: Relative LF harmonic distortion of all three PVInvs in very low power mode and for WF1 and ZS1 is around 20-40 times higher than the corresponding values at their rated powers (e.g. PVInv-A increases $THDS_{ILF}$ from around 2% to around 80%). The presence of source impedance (ZS2) and supply voltage distortions (WF2 and WF3) has further strong impact on two PVInvs and somewhat smaller, but still noticeable impact on the third PVInv. For example, $THDS_{ILF}$ of PVInv-B reaches 500% at SI of 5%, while at SI of 100% its reference $THDS_{ILF}$ value (for WF1 and ZS1) is around 2%.

After an initial decrease of absolute LF harmonic emissions with reduced operating power, two PVInvs start to increase their $THCS_{ILF}$ values in very low power mode (for WF1 and ZS1). Absolute harmonic emission of PVInv-A at SI of 5% is close to its emission at rated power, while absolute harmonic emission of PVInv-B at SI of 5% is close to its emission at 50% of rated power. In case of PVInv-C, however, there is no increase of absolute harmonic emission in low power mode. The presence of background voltage distortions (WF2 and WF3) and source impedance (ZS2) has strong impact on absolute emission of LF harmonics of two PVInvs: PVInv-A and PVInv-B have almost constant (i.e. power independent) $THCS_{ILF}$ values for WF2/WF3 and ZS2, which are around 2-10 times higher than reference $THCS_{ILF}$ values (for WF1 and ZS1 at rated power). In other words, PVInv-A and, particularly, PVInv-B in low power mode produce predominantly LF harmonic currents, with very small contribution from fundamental current. This can be explained after processing individual harmonic results and identifying the sign of the harmonic active powers, which changes from positive to negative, indicating that PVInv starts to behave as a passive load due to the presence of BG distortion.

2) LF interharmonics: Power-dependent interharmonic emission of all three PVInvs in LF range is similar to their power-dependent harmonic performance: $TIHDS_{ILF}$ values increase around 10-30 times in very low power mode, compared to reference $TIHDS_{ILF}$ value at rated power. The impact of the combined effects of supply voltage distortions (WF2 and WF3) and maximum expected source impedance (ZS2) on relative interharmonic emissions in LF range is smaller, but still visible. Additionally, two of three tested PVInvs have higher absolute emission of interharmonics when operating at powers lower than the rated one (PVInv-B at 75% of rated power and PVInv-C at 20% of rated power, i.e. in very low power mode).

The distorted voltage waveforms in tests (WF2 and WF3) included only LF harmonics and a specific test with an interharmonic background distortion (i.e. a ripple control signal) was also performed. This test has shown that interharmonic emission will increase if an interharmonic background distortion is present together with source impedance. Due to the space limitation, however, these results are not reported in this paper.

3) HF harmonics and interharmonics: For WF1 and ZS1, relative HF harmonic and interharmonic distortion of all three PVInvs in very low power mode increases around 10-30 times in comparison to the corresponding values at their rated powers (e.g. $TH\&IHDS_{IHF}$ value at 5% SI of PVInv-C is around 30%, compared to around 1% at SI of 100%). Power-dependent changes of absolute HF components are generally less pronounced and show continuous reduction of $TH\&IHCS_{IHF}$ values with reduced operating powers. With respect to emission of HF components for WF1 and ZS1, all PVInvs reduce their HF emissions for ZS2 and WF2/WF3, due to a strong damping effect of the introduced relatively high value of the source impedance ZS2. Absolute HF distortion emission of PVInv-C for WF1 and ZS1, which is slightly lower than its absolute LF harmonic emission at rated power, becomes twice higher in very low power mode. In other words, predominant part of its output current in very low power mode are HF harmonics and interharmonics. On the other hand, PVInv-B has twice higher absolute emission of HF harmonics and interharmonics than LF harmonics at rated power, the two are equal in low power mode, while in very low power mode HF emission is somewhat lower than LF harmonic emission. PVInv-A, however, has no strong emission of HF components in the considered frequency range.

Basically, the results for low and very low operating powers clearly demonstrate inability of PVInvs' control circuits to maintain low levels of harmonic and interharmonic emissions specified by manufacturers for rated operating powers for compliance with standard limits, particularly when background voltage distortion and source impedance are present. The likely reason for this seems to be related to the changes in PVInvs' control in cases of low SI levels (lower than 25%) with respect to higher SI levels (from 25% to 100%). This is subject of further investigation by the authors, as the exact information on PVInv's control is currently not available. However, this paper shows preliminary results of the impact of MPPT control on LF interharmonic emission of tested PVInvs, which was evaluated using the available measurements of dc currents and voltages at the output of PV emulator (i.e. input of PVInv).

V. Interharmonics due to MPPT Control

This section deals with the origins and causes of previously presented and discussed interharmonic emissions of PVInvs and critically analyzes the assessment of interharmonic distortion based on individual and standardized measurement methods.

A. *Origin of Interharmonic Emission*

It is well known that one of the main origins of interharmonic distortions is related to the non-synchronous behavior of two electrical sub-systems interconnected through a power electronic interface [24]. In the case of a typical grid-connected PV plant, these two sub-systems are constituted by the PV panel and related dc-dc converter on the one side, and by electrical grid, on the other. The first sub-system is a time-varying system represented by a continuous action of the MPPT control of the dc-dc converter, which effectively tries to extract the maximum possible power from the PV panels for each input solar irradiance level, corresponding to specific operating point. The second sub-system is synchronized with the grid fundamental frequency. The dc-ac PV inverter interfaces these two sub-systems producing interharmonic emission which is so far neither reported nor analyzed in the existing literature.

On the other hand, the variations in the ac power output due to the dc-ac PWM inverter control for various grid supply conditions and input dc power adjusted by the MPPT control are well-known and analyzed to a large extent in the literature with reference to harmonic emission.

Fig. 13 illustrates measured instantaneous dc power versus dc voltage of PVInv-B for ideally sinusoidal supply voltage (WF1) and ZS2 for different solar irradiance (SI) levels. These results show that the dc voltage is continuously adjusted by the MPPT control algorithm. The adjusted extraction of maximum power by MPPT control for lower input solar irradiance levels is characterized by a "slower dynamic" (i.e. lower frequency variations of dc voltage) due to the increased "flatness" of P-V curve of the panel. This is further illustrated in a smaller inset plot in Fig. 13, which clearly shows differences between the P-V curves for 100% and 10% SI levels, with the latter being more difficult for MPPT control adjustment.

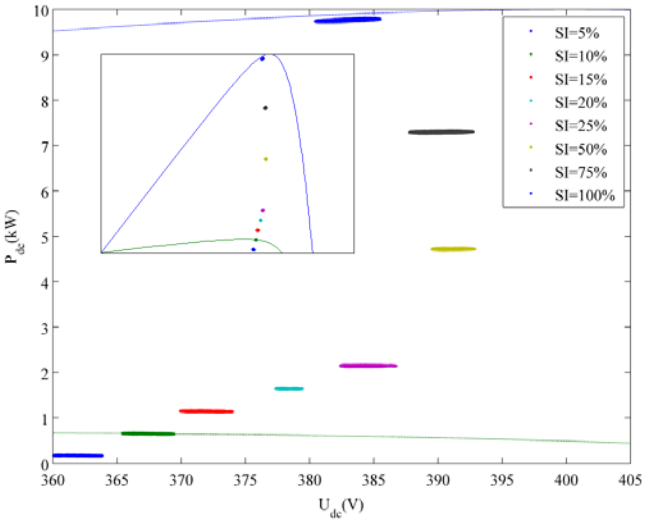

Fig. 13. Measured instantaneous dc power versus dc voltage of PVInv-B for WF1, ZS2 and different SI levels (inset plot shows full P-V curves for 100% and 10% SI levels).

Fig. 14a shows the PVInv-B instantaneous dc voltage for the SI level of 75% (when it produces highest interharmonic emission) and period of operation between 0-2 seconds. Figs. 14b and 14c show the corresponding instantaneous ac voltage and ac current outputs, respectively.

Fig. 14a demonstrates that the operational variations of the PVInv-B input dc voltage are characterized by the two dominant modes/frequencies due to the actions of the MPPT searching algorithm. The first mode has a period of around 0.03 s, i.e. frequency of around 33.3 Hz, while the second mode has a period of around 0.5 s, i.e. frequency of around 2 Hz. The high value of the fundamental voltage component does not allow clear identification of any of the two modes in Fig. 14b, but Fig. 14c clearly shows that the output ac current is modulated due to the non linear transfer of the spectral components (at multiples of the 2 Hz) from the input side to the output side of PVInv, explaining the presence of interharmonic distortion in Figs. 7-12.

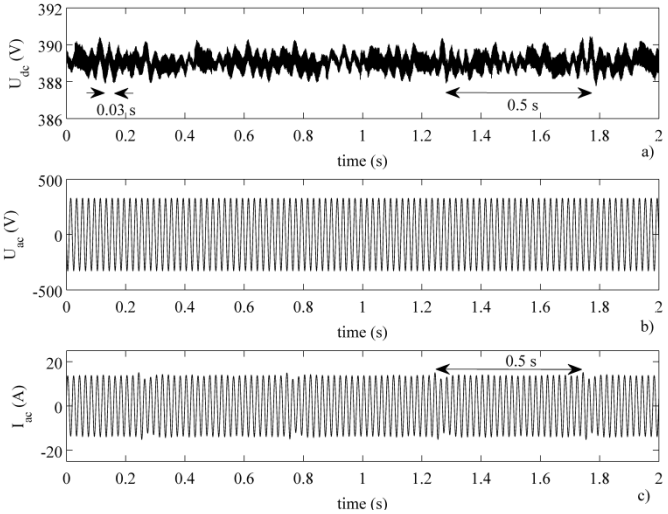

Fig. 14. Variations in the instantaneous input dc voltage (a), output ac voltage (b) and output ac current (c) of PVInv-B for WF1, ZS2 and SI of 75%.

B. Assessment Based on Individual Measurement Methods

Fig. 15 presents the processed spectra of the three signals from Fig. 14, obtained by means of a very accurate algorithm proposed previously by some of the authors for extracting the interharmonic content from a distorted signal in [25]. The used interharmonic assessment approach is based on a Double-Stage (DS) procedure: at the first stage, the actual frequencies, amplitudes and phase angles of the fundamental and harmonic frequencies are estimated using an interpolation procedure in the frequency domain, allowing to filter-out (i.e. subtract) the estimated fundamental and harmonic components from the original signal. At the second stage, the interharmonic components of the signal filtered in the first stage are evaluated without (or with strongly reduced) spectral leakage due to desynchronization problems. The need of applying this algorithm is related to a slight desynchronization of the fundamental component, whose frequency measured during the test was 49.994 ± 0.001 Hz.

The amplitude modulation of the input dc voltage due to MPPT is evident in Fig. 15a, where the spectral components at frequency distances of 2 Hz are present. Furthermore, this figure allows to observe the second modulation mode around 34 Hz. The spectral components of dc voltage highlighted in Fig. 15a are then inter-modulated by the dc-ac inverter and directly transferred to the output ac supply voltage, shown in Fig. 15b, where the presence of some interharmonics could be seen around the fundamental component. The amplitude modulation of the output ac current at the corresponding interharmonic frequencies is evident from Fig. 15c.

The assessment of the interharmonic emission of PVInvs can be done using available information on MPPT control from the measurements and by performing further DFT analysis on a 0.5 s windows, allowing to capture the 2 Hz interharmonic components.

Finally, it is worthwhile to observe that even if the amplitudes of voltage interharmonics are quite small, they are still capable of producing short-term flicker value of around Pst=0.54, as evaluated both by means of a digital implementation of an IEC Flickermeter [26] and by a commercial PQ analyzer (Pst=0.57).

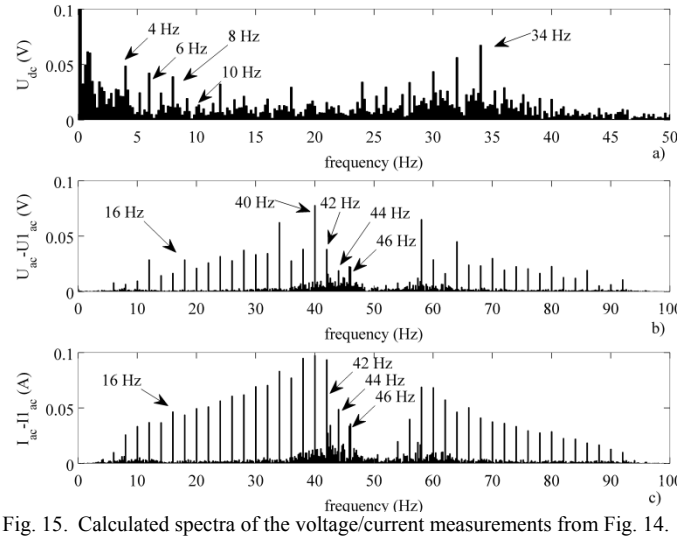

Fig. 15. Calculated spectra of the voltage/current measurements from Fig. 14.

C. Assessment Based on Standardized Measurement Methods

As discussed in the previous sub-section, the time-varying modulation of the output ac voltages and currents, caused by the action of MPPT control on input dc voltage at adjusted operating point, effectively introduces spread (leakage) of the spectrum of both voltages and ac current, This can be observed in Fig. 15, where broadband spectra are present in the frequency range from 30 to 70 Hz. In order to cope with this problem, the IEC standard [6] defines the "interharmonic subgroups" as the rms value of all interharmonic components between the two adjacent "harmonic subgroups". The amplitudes of spectral leakage components due to the desynchronization with the fundamental component, especially in the aforementioned range, can lead to inaccuracy in the calculation of interharmonic subgroups of the same order of magnitude as the interharmonics themselves. In fact, some of the authors have previously shown in that a small error in synchronization might cause remarkable spectral leakage problems for approach recommended in [6] due the use of the rectangular window. However, the accuracy of the analysis can be improved by either adopting specific enhanced synchronization hardware, or by employing suitable algorithms.

Concerning the algorithms, some of the authors have already developed some signal processing techniques that could improve overall measurement accuracy by reducing sensitivity to desynchronization [25], [27]-[28].

In order to assess the deviations in the evaluation of interharmonic subgroups between commercially available PQ instruments (IEC 61000-4-30 Class A) adopting the IEC approach and the abovementioned alternative methods, nine long time measurements (15 min) have been performed on the three PVInvs and analyzed with one commercial PQ instrument (PQI) and the alternative methods. The first three tests have been conducted assuming supply network conditions characterized by WF1 and ZS2 for a SI level of 100%. Moreover, the three tests have been repeated with adding an interharmonic of 1 % amplitude with respect to the fundamental at 375 Hz and then with adding a high frequency voltage harmonic of amplitude 1 % at 7.5 kHz.

The following text presents and discusses only the results obtained for the PVInv-B tested with WF1 and ZS2 due to space limitation.

Fig. 16a shows the comparison of the aggregated results over a 1 min period obtained by the PQI for the $TIHDS_{ULF}$ and the numerical implementations of the metric proposed in [6] (rectangular window on 10 periods (10P) of the fundamental, RW-10P), in [27] (Hanning window on 10P, HW-10P) and in [25] (Hanning window on 10P and Double Stage technique, HW-10P-DS). Fig. 16b shows the corresponding percentage deviations evaluated assuming HW-10P-DS as a reference.

A good match between the results of RW-10P and the PQI can be observed, although it is not explicitly confirmed that the algorithm implemented by the manufacturer for the IEC metric is similar to the RW-10P algorithm.

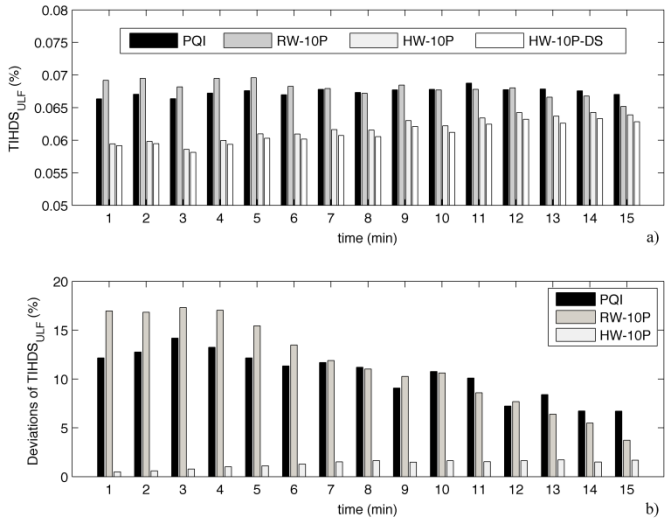

Fig. 16. Comparison of aggregated results over a period of 1 min obtained for PVInv-B (WF1 and ZS2), by means of the PQ commercial instrument (PQI) and by means of the numerical implementations of the metric proposed in [6] (RW-10P), in [27] (HW-10P) and in [25] (HW-10P-DS): a) $TIHDS_{ULF}$, b) corresponding deviations evaluated with reference to HW-10P-DS.

The mean deviation over the entire duration of the experiment is of 9%, 10% and 1.4% for PQ-Inst, RW-10P and HW-10P, respectively, showing the weakness of the approach proposed in [6] and the advantages that can be obtained by introducing the Hanning window.

Finally, Fig. 17 illustrates the possible extent and impact of the improperly handled spectral leakage problems (i.e. the inaccuracy) during the calculation of interharmonic emission of PVInv using the approach recommended in existing standards. This figure compares the deviations of the calculated $TIHDS_{ULF}$ values, obtained following (3), between the abovementioned numerical implementation of the method in [6] (RW-10P) and the technique proposed in [25] (HW-10P-DS). It could be observed that the differences in calculated voltage $TIHDS_{ULF}$ values could be very high, particularly for very low-power operating modes (corresponding to very small SI levels), reaching almost 40%.

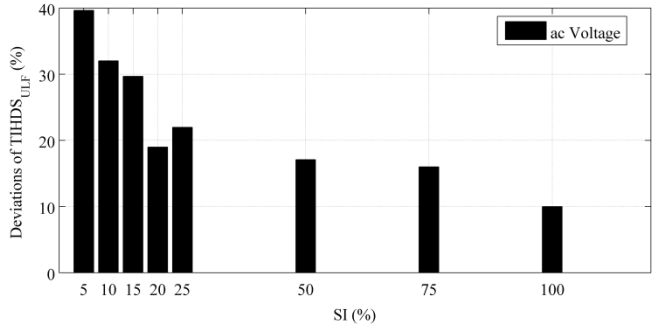

Fig. 17. Deviations of $TIHDS_{ULF}$ evaluated by means of RW-10P and HW-10P-DS vs SI for output ac voltage.

VI. Conclusions

This paper presents the results of comprehensive testing, and further analysis of obtained test results, aimed at investigating impact of operating powers and voltage supply conditions on harmonic and interharmonic emission of PVInvs. The tests have included sinusoidal voltage waveform and typical supply voltage waveform distortions, as well as minimum and maximum expected source impedance values. For evaluating harmonic and interharmonic distortion of PVInvs, both metrics recommended by existing standards and some additional indices are used. The paper has also investigated whether the MPPT control is one of the possible causes of PVInvs' interharmonic distortion.

The presented test results demonstrate that the modern PVInvs exhibit strong power-dependency of their frequency domain characteristics, indicated by a change (i.e. an increase) in both relative and absolute harmonic and interharmonic emissions in low-power operating modes (below around 25% of their rated powers), which might become particularly pronounced in very low-power operating modes (below 10% of their rated powers). Furthermore, a significant impact of combined effects of source impedance and supply voltage distortions on PVInvs' harmonic performance is identified. The presented experimental and analytical results allow to draw following conclusions and to suggest further directions of work and research:

1) Testing: The procedures for testing harmonic and interharmonic emissions of PVInvs in existing standards (e.g. [2]) should include not just the rated power and few higher power levels, but also low and very low operating powers. It could be recommended that PVInvs are tested at 5% and 10% of their rated powers. These tests should also include typically distorted voltage waveforms, e.g. similar to those used in this paper, as their impact on PVInvs behaviour could be very strong. Some of these waveforms are suggested for testing in [2], but a more systematic specification might be needed in cases when tested PVInvs exhibit strong dependency of their characteristics on background distortion voltages. An example of a test with dynamic changes of SI indicated significant increase of harmonic and interharmonic emission (resulting in tripping of tested PVInv), suggesting that similar tests could be required in cases when PVInvs are sensitive and exposed to dynamic SI conditions during the operation,

Additional impact of source impedance should be carefully considered both in the related tests (testing without impedance and with too high impedance may result in very different test evaluations) and in the related field studies (as source impedance values can vary widely in actual networks [29]).

The presented test results indicate that some PVInvs might have strong HF components emission in low power modes and/or at rated and higher powers. Accordingly, it is suggested that tests of PVInvs include HF range and use suitable HF distortion indices (e.g. $TH\&IHD_{IHF}$ and $TH\&IHC_{IHF}$).

The weakness of the approach proposed in relevant standards to assess interharmonic distortion has been disussed and the advantages that can be obtained by introducing the Hanning window have been highlighted.

2) Practical applications: Typical voltage supply conditions in modern LV networks are characterized by various levels of waveform distortions, meaning that general

assessment of power-dependent harmonic and interharmonic PVInv performance should take these conditions into account, in order to provide relevant information for practical implementation cases. Either tests or validated models of PVInvs should be used in these cases.

An additional issue is comparison of laboratory and field measurements in cases of the same and different source impedance values, which also has to be considered during the analysis. Again, one solution is to test PVInvs for a number of source impedances, covering wide range of practical values, while another is to analyze effects of different source impedance values in simulations with suitable PVInv models connected to realistic grid representations.

Finally, all results in this paper are obtained in tests with individual PVInvs. In practice, a number of PVInvs may be, and typically is connected to the same LV network and some already strong effects might be further amplified, or attenuated due to their coordinated operation (in local LV network, all PVInvs will be most likely exposed to same/similar SI levels). These situations and related issues will be very difficult to emulate in laboratory tests, but either field tests or simulations might be used for related analysis.

3) Further work: It is currently not clear what are the exact causes and origins of the presented power-dependent changes in PVInvs' performance. This should be investigated further, in order to provide suitable modifications and improvements in PVInv design, or apply appropriate network mitigation measures to prevent negative impact on both the grid and operation of other equipment connected with PVInvs.

Recommended measurement and analytical procedures for evaluating and calculating relevant performance indicators should be checked, in order to ensure that indicated high harmonic and especially interharmonic emission levels of PVInvs are correctly assessed.

The presented results include an initial investigation of the possible impact of maximum power point tracking (MPPT) control on the variations of input dc voltages in low-power operating modes, when an increased "flatness" of the panels' P-V curve might have particularly strong impact. These variations are transferred into the output ac currents by the PV inverter, which acts as a modulator, ultimately producing interharmonic emissions. To the best of the authors' knowledge, there is currently no indication of these phenomena in existing literature. Further work should include a more detailed investigation of the PVInv's controls, including MPPT of input dc current/voltage and regulation of output ac current/voltage.

APPENDIX A

TABLE A.I. SPECIFICATION OF TWO DISTORTED VOLTAGE WAVEFORMS USED IN TESTS.

"Pointed-top" Voltage Waveform		
Frequency	**RMS-Value in V**	**Phase angle in (°)**
50	229.85	0
250	6.62	0
350	4.73	180
550	1.44	180

"Flat-top" Voltage Waveform		
Frequency	**RMS-Value in (V)**	**Phase angle in (°)**
50	229.89	0
150	5.45	0
250	3.83	180
350	2.04	0
450	0.57	180
550	0.31	180
650	0.56	0
750	0.38	180
850	0.05	0
950	0.18	0
1050	0.22	180
1150	0.11	0
1250	0.04	0
1350	0.12	180
1450	0.11	0
1550	0.02	180

REFERENCES

[1] World Energy Council. "World Energy Perspective: Cost of Energy Technologies". Bloomberg New Energy Finance BNEF/WEC report prepared for presentation at the 22nd World Energy Congress in Daegu. Korea. 2013.

[2] IEC TR. Electromagnetic compatibility (EMC)–Part 3-15: Limits–Assessment of low frequency electromagnetic immunity and emission requirements for dispersed generation systems in LV networks. IEC Technical Report 61000-3-15. 2011.

[3] F. Vignola. F Mavromatakis. and J. Krumsick. "Performance of PV Inverters". *Proc. of the 37th ASES Annual Conference*. San Diego CA. 2008.

[4] S. Djokic. J. Meyer. F. Möller. R. Langella. A. Testa. "Impact of Operating Conditions on Harmonic and Interharmonic Emission of PV Inverters" *IEEE Int. Workshop on Applied Measurement in Power System* (AMPS 2015). 23-25 September 2015. Aachen. Germany.

[5] D. Perera. P. Ciufo. L. G. Meegahapola. and S. Perera. "Power quality emission assessment of photovoltaic inverters based on IEC Technical Report 61000-3-15:2011." *Australasian Universities Power Engineering Conference* (AUPEC 2013). Sept. 29 -Oct. 3 2013, Hobart, TAS.

[6] IEC. Electromagnetic compatibility (EMC). Part 4-7: General guide on harmonics and interharmonics measurements for power supply systems and equipment connected thereto. IEC Std. 61000-4-7. Ed. 2. 2009.

[7] D. Gallo. R. Langella. A. Testa. J. C. Hernández. I. Papič. B. Blažič. J. Meyer. "Case studies on large PV plants: Harmonic distortion. unbalance and their effects". *IEEE PES GM*. 21-25 July 2013. Vancouver, BC.

[8] PV Emulator (PVS 10000) http://www.spitzenberger.de/weblink/1056

[9] Power Amplifier (PAS 45000): http://www.spitzenberger.de/weblink/1002 and http://www.spitzenberger.de/weblink/1095

[10] Line impedance (AIP 75/3/P): http://spitzenberger.de/weblink/1169.

[11] Data Acquisition System: http://www.dewamerica.com/resources/Manuals/modules_manual.pdf

[12] Voltage modules (HSI-HV): https://ccc.dewetron.com/dl/53970d9a-fc10-44f0-a97f-0709d9c49861.

[13] Current modules (HSI-LV): https://ccc.dewetron.com/dl/53970d9a-05e0-44f1-b968-0709d9c49861.

[14] JCGM 101:2008: Evaluation of measurement data — Supplement 1 to the "Guide to the expression of uncertainty in measurement" — Propagation of distributions using a Monte Carlo method, First edition 2008.

[15] Current transducers (PNA-Clamp-150-DC): http://www.dewesolutions.sg/uploads/7/7/1/6/7716986/dewetron-apps_power_pm_de_b090315e.pdf.

[16] DAQ board (DEWE-ORION-0816-100X): http://www.systemtech.se/fileadmin/resources/datasheets/dewetron/2011/dewetron_dewe-orion_e.pdf.

[17] D. Gallo, C. Landi, M. Luiso, "Real-Time Digital Compensation of Current Transformers Over a Wide Frequency Range", Instrumentation and Measurement, IEEE Transactions on, Vol. 59, Issue 5, pp. 1119 - 1126, 2010.

[18] http://it.mathworks.com/help/stats/adtest.html

[19] C. De Capua , C. Landi and G. C. Malafronte "Measurement uncertainty in evaluating total harmonic distortion factor", Proc. IEEE IMTC, pp.675 -679, 2001.

[20] IEC TR. Consideration of Reference Impedances and Public Supply of Network Impedance for Use in Determining Disturbance Characteristics of Electrical Equipment Having a Rated Current Less Than 75A Per Phase. IEC Technical Report 60725. 2005.

[21] IEC. Electromagnetic compatibility (EMC). Part 4-30: Testing and Measurement Techniques – Power Quality Measurement Methods. IEC Std. 61000-4-30. Ed. 3. 2015.

[22] D. Gallo, C. Landi, M. Luiso, "AC and DC Power Quality of Photovoltaic Systems", *Instrumentation and Measurement Technology Conference*, May 13-16, 2012, Graz, Austria.

[23] S. Müller. J. Meyer. P. Schegner: "Characterization of Small Photovoltaic Inverters for Harmonic Modeling". *Int. Conf. on Harmonics and Quality of Power* (ICHQP 2014). June 2014. Bucharest. Romania.

[24] Testa A. (editor). Langella R. and IEEE Task Force on Harmonics Modeling and Simulation. "Interharmonics: theory and modeling". *IEEE Trans. on Power Deliv.* Vol. 22. pp. 2335–2348. October 2007.

[25] D. Gallo. R. Langella. A. Testa. "Desynchronized processing technique for harmonic and interharmonic analysis". *IEEE Trans. on Power Delivery*. vol. 19. no. 3. July 2004.

[26] L. Feola, R. Langella, A. Testa, "A new frequency approach for light flicker evaluation in electric power systems", *EURASIP Journal on Advances in Signal Processing*, Volume 85: 2015.

[27] D.Gallo. R.Langella. A.Testa. "On the Processing of Harmonics and Interharmonics: Using Hanning Window in Standard Framework". *IEEE Trans. on Power Delivery*. Vol. 19. N. 1. Jan. 2004.

[28] D.Gallo. R.Langella. A.Testa. "A Self tuning Harmonic and Interharmonic Processing Technique". *European Transaction on Electrical Power*. Vol. 12. N. 1. Jan./Feb. 2002. pp. 25-31.

[29] R. Stiegler, D. Chakravorty, J. Meyer, P. Schegner, "Measurement of Network Harmonic Impedance in Presence of Electronic Equipment", *IEEE Int. Workshop on Applied Measurements for Power Systems* (AMPS 2015), Aachen, 23-25. September 2015.